International Society for Rock Mechanics and Rock Engineering
Norwegian Group for Rock Mechanics

ISRM International Symposium
Eurock 2025 – Expanding the Underground Space
Trondheim, Norway, 16-20 June
ISBN 978-82-8208-079-8

Unlocking Precision in Carbon Sequestration Monitoring: Advanced Lab-Scale Monitoring of CO_2 Saturation with Combined Acoustic and Resistivity Measurement.

Kanitthorn Adisornsupawat, Anusarn Sangnimnuan
PTT Exploration and Production, Bangkok, Thailand
kanitthorna@pttep.com (email of corresponding author)

Sudarshan Govindarajan, Akshay Thombare, Munir Aldin
MetaRock Laboratories, Houston, Texas, U.S.A.

Abstract

This study investigates advanced monitoring techniques for injected CO_2 in subsurface reservoirs using simultaneous acoustic velocity and electrical resistivity measurements. Experiments were conducted on Gulf of Thailand reservoir core samples, where supercritical CO_2 was injected into brine-saturated sandstone.

The dual-measurement approach enabled continuous tracking of CO_2 migration. Brine reinjection simulated CO_2 displacement, with periodic resistivity and P-wave velocity data collection. Applying resistivity indices and Gassmann equations, the study analysed CO_2 saturation changes during drainage and imbibition. Findings contribute to improving 4D seismic monitoring and enhancing carbon sequestration strategies.

Keywords

CO_2 saturation, MMV, CO_2 laboratory, Gulf of Thailand, CCS

1 Introduction

Monitoring CO_2 plumes in Carbon Capture, Utilization, and Storage (CCUS) projects is crucial for ensuring the safety, efficiency, and long-term success of these technologies. Accurate monitoring enables verification of CO_2 injection, detection of potential leaks, and tracking of plume movement within the storage formation. Advanced methods like seismic imaging, pressure monitoring, and geochemical analysis are commonly used to track CO_2 flow and its interactions with the subsurface. Effective monitoring programs improve operational performance and help build stakeholder trust by demonstrating adherence to environmental and regulatory standards.

This study aims to determine the appropriate relationship between compressional wave velocity and CO_2 saturation changes by collecting actual samples from the planned subsurface CO_2 storage in the Gulf of Thailand. Only sidewall core samples are available for this study. Although sidewall cores are more limited in terms of sample orientation compared to conventional cores, the results obtained are consistent and can be used for future measurement, monitoring, and validation (MMV) plans.

2 Theoretical background

2.1 The impact of pore fluid on seismic properties

The seismic response is primarily influenced by compressional (V_p) and shear (V_s) velocities, as well as density. As water saturation increases, the P-wave velocity (V_p) experiences a slight increase, while the S-wave velocity (V_s) slightly decreases. However, neither V_p nor V_s alone serves as the best indicator of fluid saturation effects due to the interdependence between P- and S-waves through the shear modulus and bulk density (ρ) as shown in Eq.1 and Eq.2

$$V_p = \sqrt{\frac{K + 4G/3}{\rho}} \tag{1}$$

$$V_s = \sqrt{\frac{G}{\rho}} \tag{2}$$

Where K Bulk modulus
G Shear modulus

2.1.1 Rock properties

The bulk modulus of an isotropic rock is defined as the ratio of the hydrostatic stress to the volumetric strain. Bulk modulus values can be obtained either by laboratory measurements or analysis of wireline logs (e.g. sonic logs). See Eq.3 for the relationship below relates the bulk modulus of the rock to its compressional velocity, shear velocity and bulk density.

$$K = \rho_b \left(V_p^2 - \frac{4}{3} V_s^2 \right) \tag{3}$$

Where ρ_b Bulk density
V_p Compressional wave velocity
V_s Shear wave velocity

If we use ρ_b, V_p and V_s from the log analysis, the calculated bulk modulus will represent K_{sat}, the bulk modulus of the rock with the in-situ pore-filling fluid, but if we use ρ_b, V_p and V_s from lab measurements of a dried core sample, and the calculated bulk modulus will represent K.

The shear modulus, G, is defined as the ratio of shear stress to shear strain and is giving by Eq.4

$$G = \sigma_b V_s^2 \tag{4}$$

ρ_b and V_s can also be determined by log analysis or lab measurements, but the shear modulus is not sensitive to the fluid filling the pores, meaning means that $G_{sat} = G$ (Biot, 1956). The bulk modulus is sensitive to pore-fluid composition, while the shear modulus is not, therefore, the shear modulus will not change during the fluid substitution. This is the fundamental concept to the application of Gassmann's equation.

For the bulk density, ρ_b, the relationship below relates the porosity ($\emptyset$), fluid density (ρ_f) and the grain (matrix) density (ρ_g) and allows us to calculate ρ_b:

2.1.2 Fluid properties

The pore space in a reservoir rock is generally filled with two or more fluid phases. To analyze this, the bulk modulus and density of each fluid are computed first, and then the properties of the fluid mixture. A key assumption of Gassmann's equation is that the pores are connected, and the pressure is balanced, meaning the fluid is evenly distributed throughout the pore space. With this assumption, the bulk modulus is shown in Eq.5

$$K_f = \left[\sum_{i=1}^{n} \frac{S_i}{K_i}\right]^{-1} \quad (5)$$

Where K_f Bulk modulus of the fluid mixture
K_i Bulk modulus of the individual phases
S_i Saturation

For hydrocarbon-water system, Eq.5 is rewrite to Eq.6

$$K_f = \left[\frac{S_w}{K_w} + \frac{(1 - S_w)}{K_{hc}}\right]^{-1} \quad (6)$$

Where S_w Water saturation
K_w Bulk modulus of water
K_{hc} Bulk modulus of hydrocarbon

The density of a fluid mixture can be calculated from Eq.7

$$\rho_f = \sum_{i=1}^{n} S_i \rho_i \quad (7)$$

Where ρ_i Density of individual component

Similar to bulk modulus of fluid mixture, fluid density of a simple hydrocarbon-water system becomes Eq.8

$$\rho_f = S_w \rho_w + (1 - S_w)\rho_{hc} \quad (8)$$

Where ρ_w Density of water
ρ_{hc} Density of hydrocarbon

2.2 CO_2 saturation based on compressional velocity

Injecting CO_2 into a porous rock alters its petrophysical properties, resulting in changes to its seismic wave velocities. To describe these variations in seismic velocity, Gassmann's formulation was applied as it is straightforward and requires simple input parameters that can either be directly measured from logs or estimated based on the rock type. This model calculates seismic velocities based on the bulk modulus, which is highly sensitive to changes in fluid saturation (Han & Batzle 2004).

Since the shear modulus of fluid is zero, shear modulus of saturated rock (G_{sat}) is dependent only on the shear modulus of dry rock (G_d) is shown in Eq.9

$$G_{sat} = G_d \quad (9)$$

The density of a saturated rock (ρ_{sat}) for a given value of porosity ($\emptyset$) can be calculated from Eq.10

$$\rho_{sat} = \rho_d + \emptyset\rho_f \quad (9)$$

Where ρ_f Density of fluid

The V_p of a saturated rock (V_{psat}) can be calculated based on the saturated bulk modulus (K_{sat}), the shear modulus (G_{sat}) and the density (ρ_{sat}) of the saturated rock as shown in Eq.10

$$V_{psat} = \sqrt{\frac{K_{sat} + 4G_{sat}/3}{\rho_{sat}}} \quad (10)$$

Gassmann's equations related the saturated bulk modulus of the rock to its porosity, the bulk modulus of the porous rock frame, the bulk modulus of the mineral matrix and the bulk modulus of the pore-filling fluids as shown in Eq.11

$$K_{sat} = K_d + \frac{(1 - \frac{K_d}{K_m})^2}{\frac{\emptyset}{K_f} + \frac{1 - \emptyset}{K_m} - \frac{K_d}{K_m^2}} \tag{11}$$

Where K_d Bulk modulus of dry rock
K_m Bulk modulus of solid matrix
K_f Bulk modulus of pore fluid

Since porosity, density and moduli including K_d, K_m and G_d of a core are known or measured before the experiment, calculated V_p can be obtained after computing the values of K_f and ρ_f of the core.

3 Experiment overview

The advanced triaxial apparatus safely contains supercritical CO_2 at pressures up to 30,000 psi. It features a servo-mechanical frame press for applying deviatoric stress within a temperature-controlled enclosure. High-resolution servo-mechanical pumps regulate confining and pore pressures, with precise digital transducers ensuring accuracy. CO_2-resistant materials enhance durability, and the pore pressure pumps handle both brine and CO_2. A gas booster pump assists rapid CO2 injection, while heater jackets maintain temperatures up to 150°C. The system includes resistivity and acoustic monitoring, with all parameters tracked via a control panel.

Fig. 1 shows the step rate test setup, where supercritical CO_2 is injected from the top and brine from the bottom, with a constant differential pressure enabling flow. The confining pump simulates reservoir pressure, and heater jackets maintain in-situ temperatures. Axial force applies deviatoric stress to replicate vertical reservoir conditions. Throughout the test, CO_2 and brine pump positions, acoustic velocity, and resistivity are monitored.

Initially, resistivity stabilizes as the sample saturates with brine. A high-pressure pulse alters resistivity, and compressional velocity is recorded throughout. If CO_2 breakthrough occurs, resistivity rises at the bottom pore line due to CO_2's non-conductivity (J. Kummerow & E. Spangenberg, 2011). Injection continues until resistivity and velocity stabilize, indicating maximum CO_2 saturation.

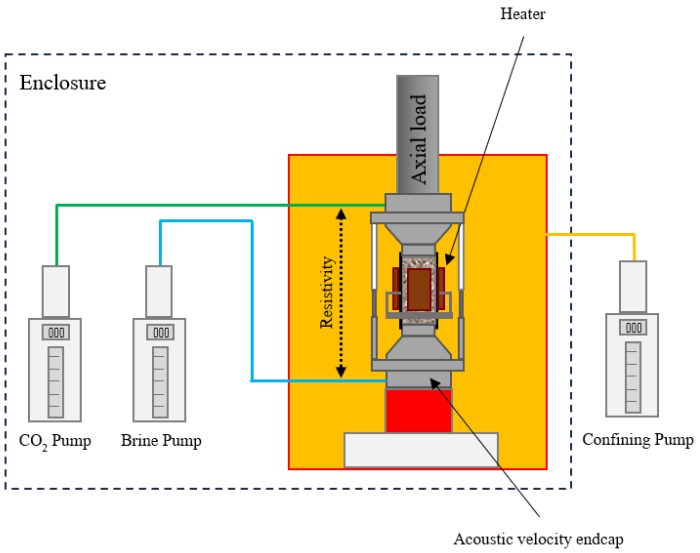

Fig. 1 Schematic diagram for the step rate test.

3.1 Experiment approach

The CO_2 fluid substitution test simulates the displacement of brine by supercritical CO_2 in a saturated rock sample under high temperatures and reservoir-representative stresses. The solubility of CO_2 and brine is a key factor in determining how much brine can be displaced by CO_2. Resistivity and acoustic signals are monitored throughout the test. The porous plate technique is used to mimic the typical distribution of fluids in reservoir rocks, providing more reliable resistivity measurements, especially at very slow injection rates. In addition to resistivity, compressional acoustic velocity is measured during the test to represent seismic monitoring in CCS projects, where acoustic velocity is widely used to track CO_2 plume migration. The relationship between compressional velocity and CO_2 saturation is expected to be established, which can be applied in the field for CO_2 monitoring.

3.2 Testing condition

In this study, four samples from different formations in the Gulf of Thailand were selected, representing potential subsurface CO_2 storage sites within the depth range of 1,600 to 2,500 m, ranging from shallow aquifers to deep depleted reservoirs. The experimental setup was designed to replicate the reservoir conditions at the specific depths from which the samples were collected. The reservoir stress state was determined using a calibrated 1-D Mechanical Earth Model (1-D MEM). In the advanced triaxial system, where the sigma 2 and sigma 3 principal stresses are assumed to be equal, the mean horizontal stress is calculated and used as the confining pressure, representing the minimum principal stress. The maximum principal stress (sigma 1) is represented by the vertical stress, which is the confining pressure plus the deviatoric stress. The initial pressure before injection is derived from the depleted reservoir or aquifer pressure. The top pump (CO_2 pump) is maintained at about 200 psi higher than the bottom pump (brine pump), with this pressure difference kept constant throughout the test. The system enclosure is maintained at an isothermal temperature of 40°C, while the heater jacket surrounding the sample can reach up to 140°C, directly transferring heat to the reservoir samples.

The selected sidewall cores were carefully quality checked using computed tomography (CT) scan images and visual inspection to ensure there were no visible fractures. Basic properties were measured, and the cores were saturated with representative formation brine prior to testing.

3.3 Laboratory testing design

The basic properties of selected 4 samples for this study is shown in Table 1. Core images for both pre and post-test condition are illustrated in Fig. 2.

Table 1 Properties of samples used in the tests.

Detail	Sample T-01	Sample T-02	Sample T-03	Sample T-04
Length (in)	1.59	1.68	1.75	1.73
Diameter (in)	1.03	1.01	1.00	1.02
Weight (g)	37.61	41.58	47.51	49.05
Bulk Volume (cc)	21.49	22.05	22.58	23.23
Grain Volume (cc)	14.03	15.74	17.91	19.12

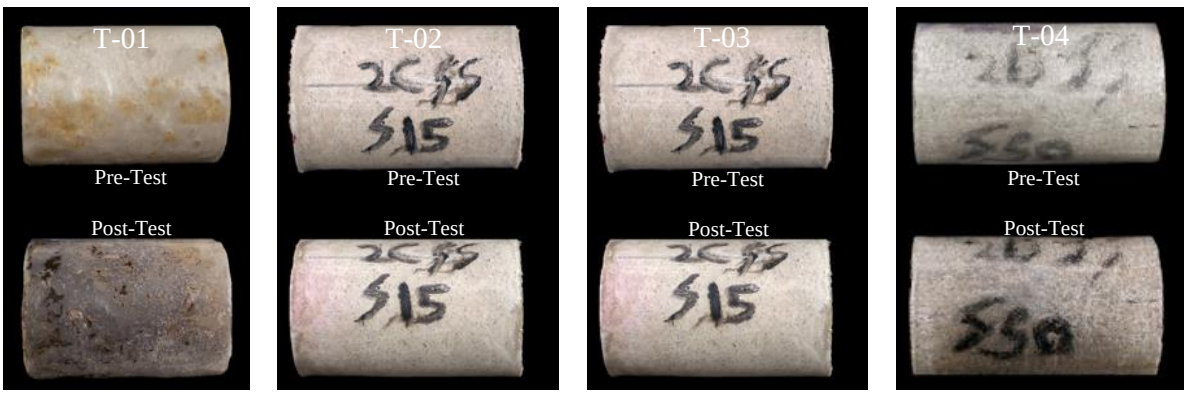

Fig. 2 Photo of experiment samples (T-01 to T-04) with Pre and Post CO_2 injection test

4 Experiment result

4.1 Variation in compressional velocity and resistivity during CO_2 injection

Fig. 7 to Fig. 10 illustrate the quality assurance process for four experiments, ranging from the shallowest CO_2 storage target with the highest porosity to the deepest target with relatively lower porosity. Four key parameters were monitored and plotted throughout the experiments to ensure consistent testing conditions across all samples.

The injected pressure, controlled by the CO_2 pump (depicted as a green solid line), and the back pressure, regulated by the brine pump (depicted as a cyan solid line), remained constant during the stabilization phase. This phase was maintained until both pressure and temperature stabilized.

The compressional wave velocity (represented by the yellow solid line) remains stable during the stabilization period until a reduction is observed as CO_2 begins to partially fill the samples.

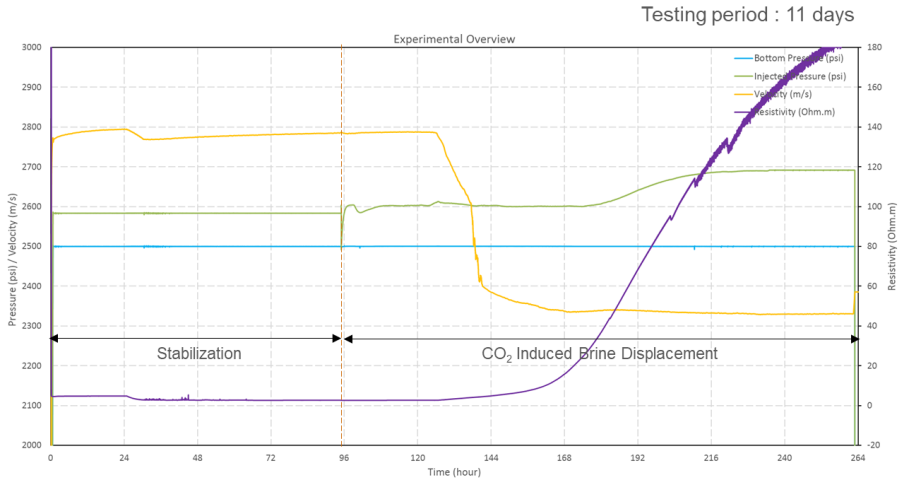

Fig. 3 Plot of pressure/velocity and resistivity through the experiment period for Sample T-01

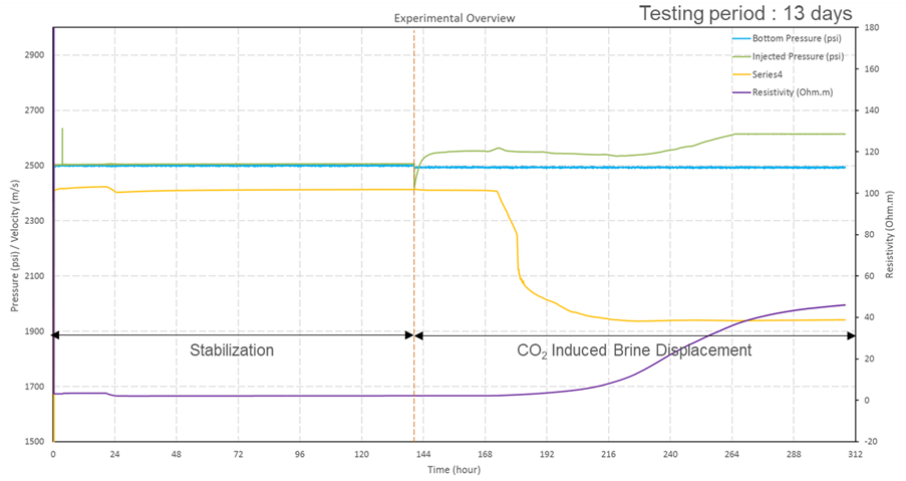

Fig. 4 Plot of pressure/velocity and resistivity through the experiment period for Sample T-02

Resistivity curve (represented by the magenta solid line) shows a slight increase at the onset of CO_2 partially filling the samples, followed by no significant change toward the end of the injection process.

It can be observed that total duration for each test ranges from 15 to 20 days, with the CO_2-induced brine displacement phase lasting less than 10 days which can be used as a baseline for CO_2 soaking period for future analysis.

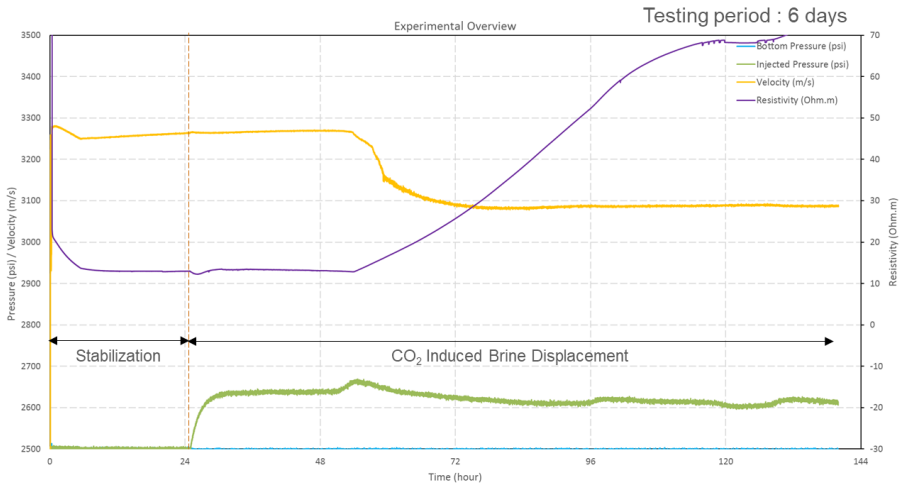

Fig. 5 Plot of pressure/velocity and resistivity through the experiment period for Sample T-03

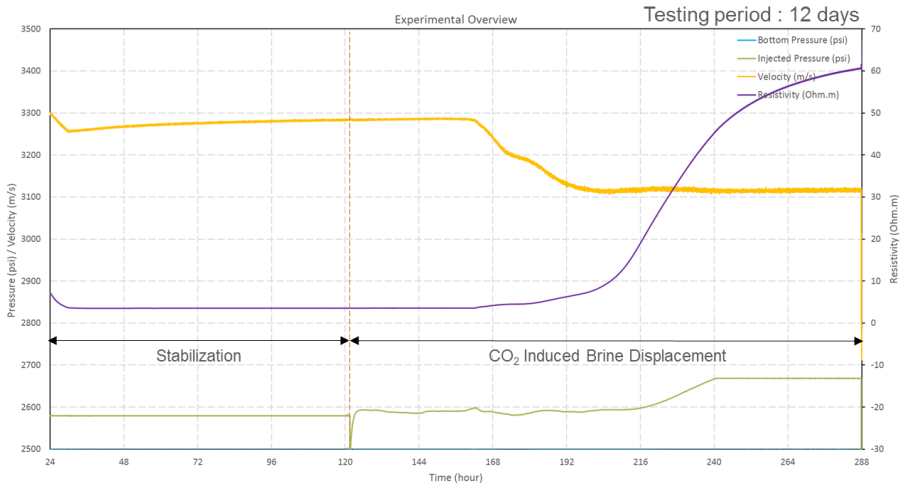

Fig. 6 Plot of pressure/velocity and resistivity through the experiment period for Sample T-04

4.2 Compressional wave velocity with CO2 saturation during injection.

Two commonly used equations to calculating the bulk modulus of two-phase immiscible fluids mixture are presented in Eq.12 for serial law and Eq.13 for parallel law.

$$K_f = S_{co2}K_{co2} + (1 - S_{co2})K_{sln} \tag{12}$$

$$\frac{1}{K_f} = \frac{S_{co2}}{K_{co2}} + \frac{1 - S_{co2}}{K_{sln}} \tag{13}$$

Where S_{co2} Saturation of CO_2
K_{co2} Bulk modulus of CO_2
K_{sln} Bulk modulus of saline

The serial law applies when the two immiscible fluids are segregated perpendicular to the direction of wave propagation, while the parallel law applies when the fluids are segregated parallel to the wave propagation direction. However, to align with regional core samples, a modification above equations is proposed. See Eq.13 and Eq.14

$$K_f = S_{sln}^n K_{sln} + (1 - S_{sln}^n)K_{co2} \tag{13}$$

$$K_f = \frac{K_{sln}K_{co2}}{K_{sln}(1 - S_{sln}^m) + K_{co2}S_{sln}^m} \tag{14}$$

Where m Modified Reuss exponent
n Modified Voigt exponent

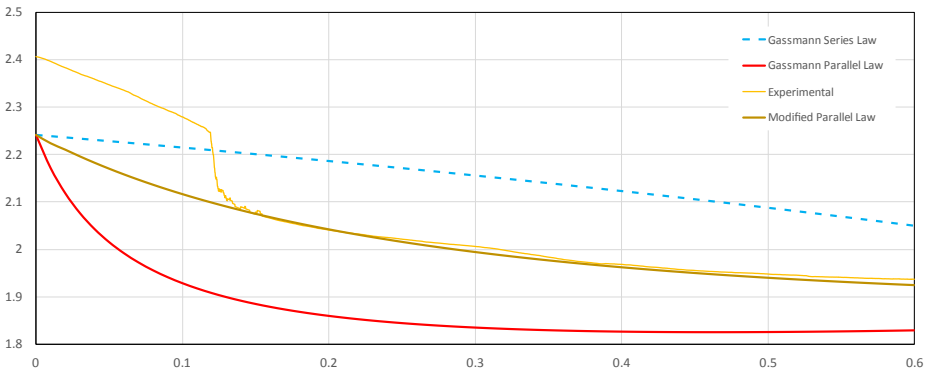

Fig. 7 Compressional wave velocity versus CO_2 saturation for Sample T-01

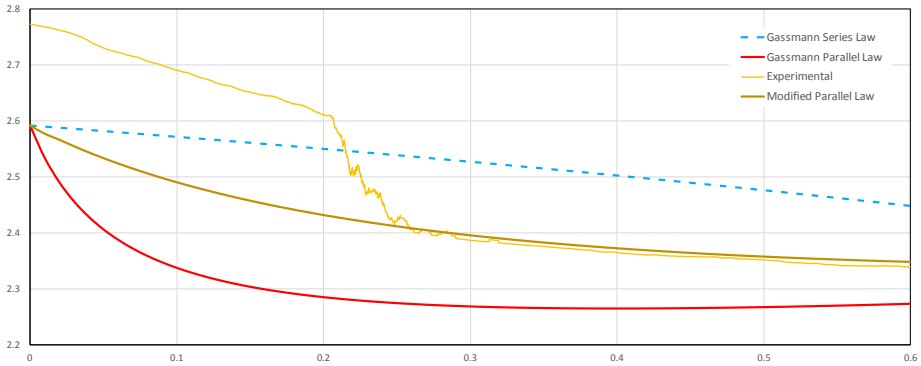

Fig. 8 Compressional wave velocity versus CO_2 saturation for Sample T-02

The plot of P-wave velocity versus CO_2 saturation for all samples are shown in Fig. 7 to Fig. 10. The y-axis represents P-wave velocity decrease as CO_2 saturation increase, which is expected since CO_2 is less dense and less stiff compared to the original fluid in the pore space. The x-axis represents CO_2 saturation. As this saturation increase, the P-wave typically decreases because CO_2 reduce the rock's bulk modulus and density. Red curves represent P-wave response following Gassmann parallel low where blud dash curve represent P-wave response following Gassmann serial law. Yellow dash curve and brown curve represent modified parameters to match with actual response of rock specimen from Gassmann parallel and serial respectively. Yellow curves represent actual P-wave response from experiment with increasing of CO_2 saturation in the sample.

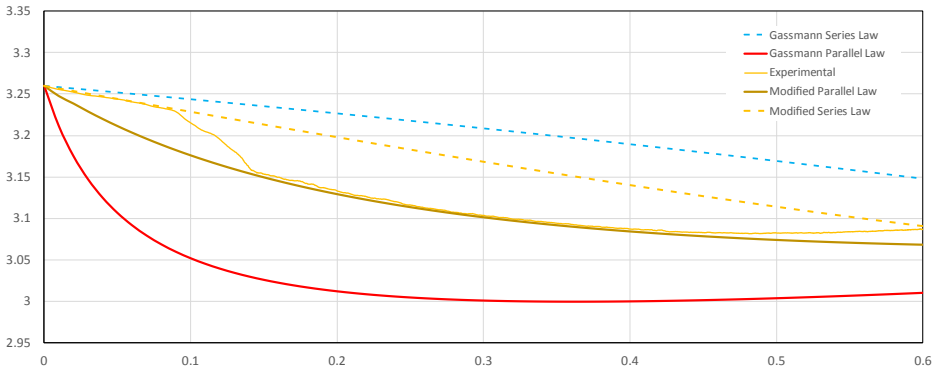

Fig. 9 Compressional wave velocity versus CO_2 saturation for Sample T-03

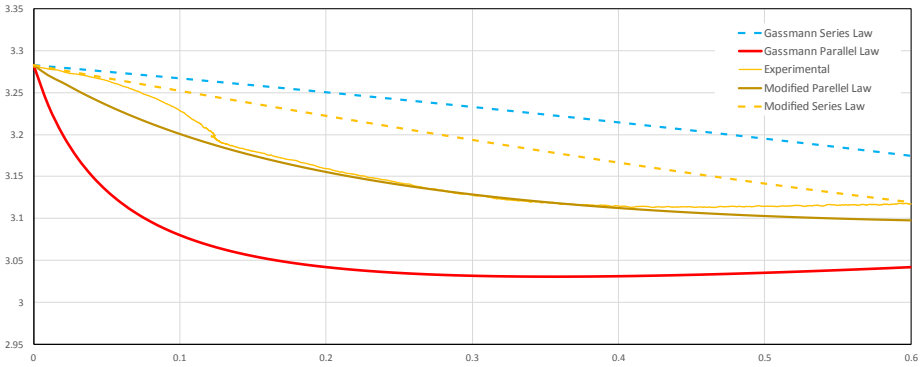

Fig. 10 Compressional wave velocity versus CO_2 saturation for Sample T-04

From this study, equation that represent bulk modulus of fluid for this region are

$$K_f = S_{sln}^{1.55} K_{sln} + \left(1 - S_{sln}^{1.55}\right) K_{co2} \tag{15}$$

$$K_f = \frac{K_{sln} K_{co2}}{K_{sln}(1 - S_{sln}^{0.22}) + K_{co2} S_{sln}^{0.22}} \tag{16}$$

4.3 Resistivity Response related to CO_2 saturation during injection.

Resistivity monitoring for understanding the saturation state of rock samples has been applied historically by geoscientists (G. Archie, 1942), (S. Govindarajan, 2023). Resistivity is a direct measure of conductive ability i.e. the ionic strength and the mobility of the ions in the fluid within the pore space. A rock sample completely saturated with high salinity pore fluid, with high ionic strength, will have high conductivity i.e. low resistivity. A decrease in ionic content i.e. expulsion of the pore fluid will be accompanied by a decrease in conductivity or increase in resistivity. Thus, when CO_2 displaces the brine within the sample there is an increase in resistivity. The increase in resistivity is proportional to the storage efficiency of CO_2 in the rock sample. In the laboratory setting, data indicates resistivity is more sensitive to saturation change than velocity. Resistivity continues to increase with brine displacement and becomes stable when there is no more brine expulsion. The magnitude of resistivity change at the end of the experiment, is indicative of CO_2 saturation achievable in the rock.

Fig. 7 to Fig. 10 depict the change in the resistivity over the course the entire experiment for each of the samples amongst other data. Data indicates T-01 has the maximum change in resistivity indicating potential for maximum storage achievement compared to the other candidates.

5 Conclusion

Injecting CO_2 into sandstone in a laboratory setting provides essential insights into fluid-rock interactions, which are vital for understanding applications such as CO_2 sequestration. Key laboratory observations include changes in pore pressure dynamics due to the distinct behaviour of CO_2 in its liquid, gas, or supercritical phases; geochemical interactions, particularly when CO_2 dissolves in water to form carbonic acid (H_2CO_3); alterations in porosity and permeability as mineral reactions modify flow pathways, potentially restricting fluid movement; and variations in mechanical properties caused by the dissolution of cementing materials. Further evaluation based on relative permeability is needed to finalize best candidate for sequestration as understanding these behaviours is critical for designing and optimizing CO_2 storage strategies.

This study focuses on both resistivity and compressional wave velocity measurement. However, for large-scale CO_2 plume monitoring, seismic velocity is more suitable due to ability to penetrate in deep reservoirs and heterogeneous formations with CO_2 migration over time. In contrast, resistivity monitoring can only be performed at the near monitoring well region with limited depth penetration and only works well conductive environments like saline aquifers. Due to the limitation of resistivity

measurement, the goal is to study the impact of compressional wave velocity and its direct correlation with CO_2 saturation levels in clastic reservoirs within the Gulf of Thailand. A critical parameter, the bulk modulus of the pore-filled fluid mixture comprising CO_2 and formation brine, is determined. The findings will contribute to the development of a Monitoring, Measurement, and Verification (MMV) strategy for tracking CO_2 plume migration and monitoring during the CO_2 injection phase of an upcoming campaign, supporting the nation's efforts toward achieving its net-zero emissions target.

References

Archie, G. E., (1942) The electrical resistivity log as an aid in determining some reservoir characteristics, Trans. AIME, 146, 54–67.

Adisornsupawat, K.; Sangnimnuan, (2023) Evaluation of Caprock Integrity with Laboratory Scale In-Situ CO_2 Injection Test; ARMA.

Batzle, M., and Wang, Z., (1992) "Seismic properties of pore fluids", Geophysics 57:1396–1408.

Berryman, J. G., (1999) "Origin of Gassmann's equations", Geophysics 64:1627–1629.

Castagna, J. P., Batzle, M. L., and Eastwood, R. L., (1985) "Relationship between compressional-wave and shear-wave velocities in clastic silicate rocks", Geophysics 50: 571–581.

Grochau, Marcos and Gurevich, Boris. (2009) "Testing Gassmann fluid substitution: sonic logs versus ultrasonic core measurements", Geophysical Prospecting

Han D., "Fluid saturation effect on rock velocities in seismic frequencies", SEG-EAGE Summer Research Workshop (1992).

Han D., Michael L. Batzle, (2004) "Gassmann's equation and fluid-saturation effects on seismic velocities", Geophysics 69: 398– 405.

J. K. Kim, J. Xue, T. Matsuoka (2010) "Experimental study on CO_2 monitoring and saturation with combine P-wave velocity and resistivity." SPE Journal, SPE 130284.

Kumar D., (2006) "A Tutorial on Gassmann Fluid Substitution", Geohorizons.

Kummerow J., Spangenberg E., (2011) "Experimental evaluation of the impact of the interactions of CO_2-SO_2, brine, and reservoir rock on petrophysical properties: A case study from the Ketzin test site, Germany, Geochemical Society

M. Gutierrez, D. Katsuki, A. Almarabat. (2020) "Seismic velocity change in sandstone during CO_2 injection. E3S Web Dof Conferences, 205, ICEGT.

Per Avseth, Tapan Mukerji and Gary Mavko, (2005) Quantitative Seismic Interpretation: Applying Rock Physics Tools to Reduce Interpretation Risk (University Press), 5-6.

Q. Shi, Z. Q. Xue, S. Durucan (2007) "Seismic monitoring and modelling of supercritical CO_2 injection into a water-saturated sandstone: Interpretation of P-wave velocity data." Int. J. Greenhouse Gas Control.

S. Govindarajan, Aldin M., Thombare A., et. al., (2023) Integrated thermo-poro-mechanical characterization for CO2 sequestration at deep aquifer conditions, E3S Web of Conference 367. https://doi.org/10.1051/e3sconf/202336701001.

Tad M. Smith, Carl H. Sondergeldz, and Chandra S. Rai, (2003) "Gassmann fluid substitutions", Geophysics 68: 430-440.